Original article

Nuclear Medicine Communications

Computed tomography-based attenuation correction in neurological positron emission tomography: evaluation of the effect of the X-ray tube voltage on quantitative analysis

Mohammad Reza Ay and Habib Zaidi

Background **The advent of dual-modality positron emission tomography/computed tomography (PET/CT) imaging has revolutionized the practice of clinical oncology by improving lesion localization and facilitating treatment planning for radiation therapy. In addition, the use of CT images for CT-based attenuation correction (CTAC) allows the overall scanning time to be decreased and a noise-free attenuation map (μmap) to be created. The most common procedure requires a piecewise linear calibration curve acquired under standard imaging conditions to convert the patient's CT image from low effective CT energy into an attenuation map at 511 keV.**

Aim **To evaluate the effect of the tube voltage on the accuracy of CTAC.**

Methods **As different tube voltages are employed in current PET/CT scanning protocols, depending on the size of the patient and the region under study, the impact of using a single calibration curve on the accuracy of CTAC for images acquired at different tube voltages was investigated through quantitative analysis of the created μmaps, generated attenuation correction factors and reconstructed neurological PET data using anthropomorphic experimental phantom and clinical studies.**

Results **For CT images acquired at 80 and 140 kVp, average relative differences of −2.9% and 0.7%, respectively, from the images acquired at 120 kVp were observed for the absolute activity concentrations in five regions of the anthropomorphic striatal phantom when CT images were converted using a single calibration curve derived at 120 kVp. Likewise, average relative differences of 1.9% and −0.6% were observed when CT images were acquired at 120 kVp and CTAC used calibration curves derived at 80 and 140 kVp, respectively.**

Conclusion **The use of a single calibration curve acquired under standard imaging conditions does not affect, to a visible or measurable extent, neurological PET images reconstructed using CTAC when CT images are acquired in different conditions.** *Nucl Med Commun* **27:339–346 © 2006 Lippincott Williams & Wilkins.**

Nuclear Medicine Communications 2006, **27**:339–346

Keywords: attenuation correction, brain imaging, PET/CT, quantification, tube voltage

Division of Nuclear Medicine, Geneva University Hospital, Geneva, Switzerland.

Correspondence to Habib Zaidi, Division of Nuclear Medicine, Geneva University Hospital, CH-1211 Geneva 4, Switzerland.
Tel: +41 22 372 7258; fax: +41 22 372 7169;
e-mail: habib.zaidi@hcuge.ch

Sponsorship: This work was supported by the Swiss National Science Foundation under grant SNSF 3152A0-102143.

Received 22 November 2005 **Accepted** 13 January 2006

Introduction

The advent of combined positron emission tomography/computed tomography (PET/CT) units is considered as a major advance in medical imaging technology and health care. As the name implies, PET/CT combines the information produced by two sophisticated imaging modalities, the functional information from PET with the anatomical information from CT, into a single procedure [1]. Dual-modality imaging correlates functional and anatomical data to improve disease localization and facilitates treatment planning for radiation oncology or surgery [2]. PET/CT systems offer significant advantages over stand-alone PET, including decreased overall scanning time and increased accuracy in lesion localization. The high-resolution anatomical information from PET/CT improves the differentiation of the physiological (normal) uptake of ^{18}F-fluorodeoxyglucose ([^{18}F]FDG) and other radiopharmaceuticals from that associated with disease, thereby reducing false-positive errors in comparison with lesion characterization using PET imaging alone.

Several physical factors can degrade the image quality and quantitative analysis of PET: the most important is photon attenuation in tissues, which can affect both the visual interpretation and quantitative analysis of PET data [3]. Several transmissionless methods (that do not require a transmission scan) have been devised to correct for attenuation in neurological PET studies [4–7]. One of the advantages of PET/CT is the ability to generate a noise-free attenuation map (μmap) to be used for attenuation correction purposes. With the introduction of hybrid PET/CT systems into the clinical setting, precise conversion from CT numbers derived from low-

0143-3636

energy polyenergetic X-ray spectra to linear attenuation coefficients at 511 keV has become essential in order to apply accurate CT-based attenuation correction (CTAC) to the PET data. Several CTAC strategies have been developed, including scaling [8], segmentation [9], hybrid segmentation/scaling [10], piecewise linear scaling [11,12] and dual-energy decomposition methods [13]. Most commercially available PET/CT scanners use the bilinear calibration curve method, which is generally calculated at a preset tube voltage (120–140 kVp) and current. Kamel *et al.* [14] investigated the effect of varying tube current, and showed that a low-current CT is sufficient for CTAC using comparative quantitative analysis of reconstructed clinical PET images. As patient CT images may be acquired at different tube voltages and currents, depending on the patient size and region under study, and considering the fact that the CT number of a particular tissue is tube voltage dependent, it was hypothesized that the use of a single calibration curve calculated at a specific tube voltage for CT images acquired under different scanning conditions might propagate a significant uncertainty during the CTAC procedure. Bai *et al.* [12] argued that the slope of the bilinear calibration curve for CT numbers higher than 0 Hounsfield units (HU) was tube voltage dependent. Other studies have reported on the relevance of deriving tube voltage-dependent CTAC schemes for PET/CT [15]. These topical developments, combined with the lack of detailed studies investigating the effect of tube voltage on the quantitative analysis of non-clinical PET data, where the ground truth is known, motivated the work presented in this paper.

This study was designed to provide answers to the following legitimate questions of the clinician or physicist: 'what is the magnitude of error of acquiring CT at, for example, 80 kVp when the calibration curve is the manufacturer's standard of 120 or 140 kVp?' or, vice versa, 'what is the magnitude of error of acquiring CT images at specific tube voltages and varying the voltage for the derivation of calibration curves'. The assessment was carried out through quantitative analysis of created μmaps, generated attenuation correction factors (ACFs) and reconstructed neurological PET data using experimental anthropomorphic phantom and clinical studies.

Materials and methods

Phantom and clinical studies

Our department is in the process of installing a commercial PET/CT scanner; however, this was not available during the actual study design, which relied on the use of PET and CT data acquired on separate PET and CT scanners. One of the motivations behind the choice of brain imaging is that automated multimodality coregistration algorithms work relatively well (in contrast with whole-body imaging) and can be applied most successfully to neurological studies, where the skull provides a rigid structure that maintains the geometrical relationship of structures within the brain. An anthropomorphic head phantom (Radiology Support Devices Inc., Long Beach, California, USA), designed specifically for the assessment of quantitative imaging capabilities of the striatum relevant for PET studies of the presynaptic and postsynaptic dopaminergic system, was employed in order to quantitatively assess the effect of using a single calibration curve on the accuracy of CTAC when CT images were acquired at different tube voltages. The phantom has five compartments which can be filled separately: left and right caudate nucleus (LCN and RCN), left and right putamen (LPU and RPU) and the rest of the brain (main chamber). The main chamber itself is embedded in a bone-like structure to provide properties similar to the human head.

For an activity ratio of 1 : 8 between the main chamber and small cavities, 2.942 MBq of ^{18}F (in 0.9 ml of 0.9% NaCl) was diluted in distilled water and used to fill the striatum. A total activity of 13.2 MBq diluted in 1.1 ml of NaCl was added to the main chamber. Subsequently, the main chamber was totally filled with distilled water. The fully three-dimensional emission study lasted 25 min, whereas a two-dimensional pre-injection transmission scan (10 min) was acquired using ^{137}Cs single-photon point sources on an ECAT ART PET scanner (CTI/Siemens, Knoxville, Tennessee, USA). This is a whole-body, three-dimensional tomograph having less than one-half the number of bismuth germanate detectors compared with a full ring scanner with the equivalent field of view, upgraded to use collimated point sources of ^{137}Cs, and is capable of producing high-quality, scatter-free data in this continuously rotating partial-ring tomograph. The measured transmission scan was scaled for the difference between 662 and 511 keV energies by normalizing to a slab phantom scan and correcting for scatter and cross-section variation using a log-linear transformation of the attenuation factors. Thereafter, CT data of the same phantom were acquired on an Aquilion CT scanner (Toshiba Medical Systems Corporation, Tokyo, Japan) at 240 mA in order to apply the CTAC procedure to the emission data. This CT scanner has 40 parallel detector rows with 35 840 detector elements, 32 mm detector length along the patient axis and offers 16 slices (0.5 mm thickness) with each 0.5 s gantry revolution. Calibration curves calculated at 80, 120 and 140 kVp were used to create sets of μmaps from images acquired at 80, 120 and 140 kVp. The emission data were corrected for attenuation using the measured transmission method (MTM) as well as the set of μmaps generated using CTAC. Apparent recovery coefficients (ARCs), representing the apparent (observed or partial volume corrected) regional radioactivity concentration to true activity ratio, and absolute activity concentrations were calculated for the five compartments of the striatal phantom as figures of merit

for the quantitative analysis of reconstructed neurological PET images.

A polyethylene cylindrical phantom ($\phi = 250 \pm 0.5$ mm), containing 16 cylindrical holes ($\phi = 20 \pm 0.5$ mm), was made in order to calculate the bilinear calibration curves required for application of the CTAC procedure. Fourteen syringes were filled with a solution of K_2HPO_4 and water, with concentrations varying between 50 and 900 mg/cm^3 to simulate cortical bone with different densities. The prepared syringes, together with two additional syringes containing water and air, were inserted into the polyethylene phantom's holes (see Fig. 1). Subsequently, the phantom was scanned on a HiSpeed X/iF CT scanner (General Electric Healthcare Technologies, Waukesha, Wisconsin, USA) using three different tube voltages (80, 120 and 140 kVp). This CT scanner uses a Highlight ($Y_2Gd_2O_3$:Eu) ceramic scintillator and has a 541 mm source to isocentre and 949 mm source to detector distances and 816 detector elements (793 active elements) with a physical dimension of 0.8 mm. The bilinear calibration curves at different tube voltages for both CT scanners were calculated according to the method proposed by Bai *et al.* [12]. Patient brain CT scans acquired at 120 kVp on the HiSpeed X/iF CT scanner were selected from the database and used for the clinical evaluation of the effect of the tube voltage.

Attenuation correction and image reconstruction

The computation of ACFs derived from CTAC involved down-sampling the CT image matrix to 128 × 128, followed by Gaussian smoothing using a 6 mm kernel, to match the spatial resolution of the PET scanner employed in this study. CT numbers (in HU) were then transformed to linear attenuation coefficients at 511 keV using the calculated bilinear curve. The created μmaps were forward projected to generate 47 ACF sinograms. The attenuation-corrected projections were reconstructed using the 3DRP reprojection algorithm implemented within ECAT 7.2.1 software (CTI Molecular Imaging Inc., Knoxville, Tennessee, USA) with a maximum acceptance angle corresponding to 17 rings and a span of 7. The default parameters used in clinical routine were applied (ramp filter; cut-off frequency, 0.35 cycles/pixel). The reconstructed images consist of 47 slices with 128 × 128 resolution and a voxel size set to 1.72 × 1.72 × 3.4 mm^3.

The acquired CT and preliminary PET images reconstructed using calculated attenuation correction were coregistered using the commercial Hermes multi-modality fusion software (Hermes multi-modality fusion software, Nuclear Diagnostics AB, Stockholm, Sweden) to limit potential artefacts arising from the misalignment of images during the CTAC procedure. The slice thickness of CT images was adjusted during the coregistration to match the thickness of PET images. To increase the accuracy of quantitative analysis, partial volume effect correction of the striatal phantom's PET images was performed using the geometric transfer matrix-based method [16], where the regions of interest (ROIs) were delineated on the CT images to allow the computation of the corrected estimates without *a priori* knowledge on any activity level. Briefly, the algorithm directly computes the degradations introduced by the limited spatial resolution of the PET scanner, as well as smoothing introduced during image backprojection, and further modulation during extraction of regional tracer concentration. In practice, these partial volume factors are computed from the simulation of noise-free regional spread function images and sampling with a user-defined set of ROIs.

Fig. 1

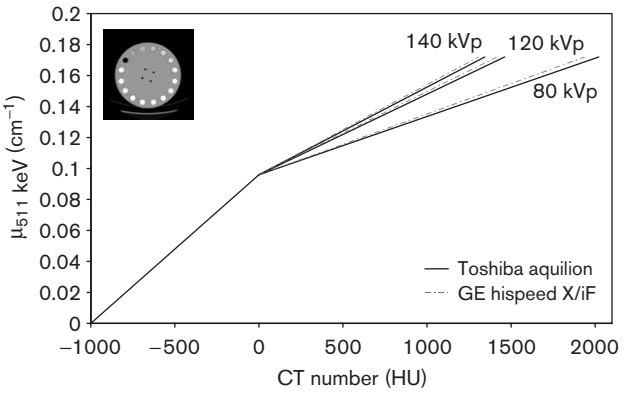

Calculated bilinear calibration curves for conversion of computed tomography (CT) numbers (Hounsfield units, HU) into linear attenuation coefficients at 511 keV at different tube voltages for both Aquilion and HiSpeed X/iF CT scanners. The in-house designed polyethylene cylindrical phantom containing 16 cylindrical holes is shown in the top left corner.

Results

Figure 1 shows the calculated bilinear calibration curves for both CT scanners used in this study at different tube voltages (80, 120 and 140 kVp). The XCOM photon cross-sections database [17] was used to calculate the corresponding linear attenuation coefficients of the inserted solutions at 511 keV. The slopes of the calibration curves for CT numbers greater than 0 HU increase with increasing tube voltage. It is worth noting that these curves have slightly different slopes for different scanners for the same tube voltage. A typical slice of the original clinical brain CT image (512 × 512 matrix), acquired at 120 kVp, is shown in Fig. 2. Three μmaps (128 × 128 matrix) were calculated from the same data set using calibration curves calculated at different tube voltages (Fig. 2). It was considered unethical to scan the patients with varying tube voltages owing to the additional radiation dose and the absence of any direct clinical

Fig. 2

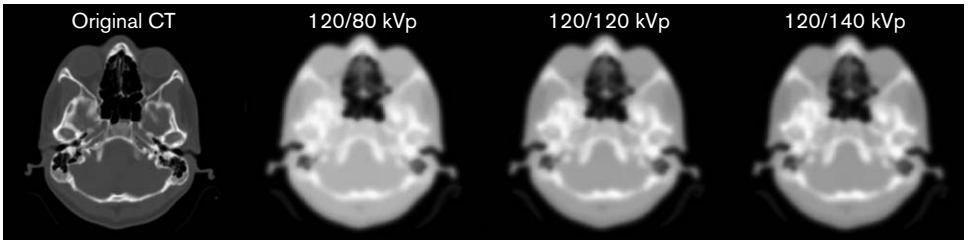

Effect of using different calibration curves during the computed tomography-based attenuation correction (CTAC) procedure. From left to right: original clinical computed tomography (CT) image acquired at 120 kVp; derived μmaps at 511 keV using calibration curves calculated at tube voltages of 80, 120 and 140 kVp.

Fig. 3

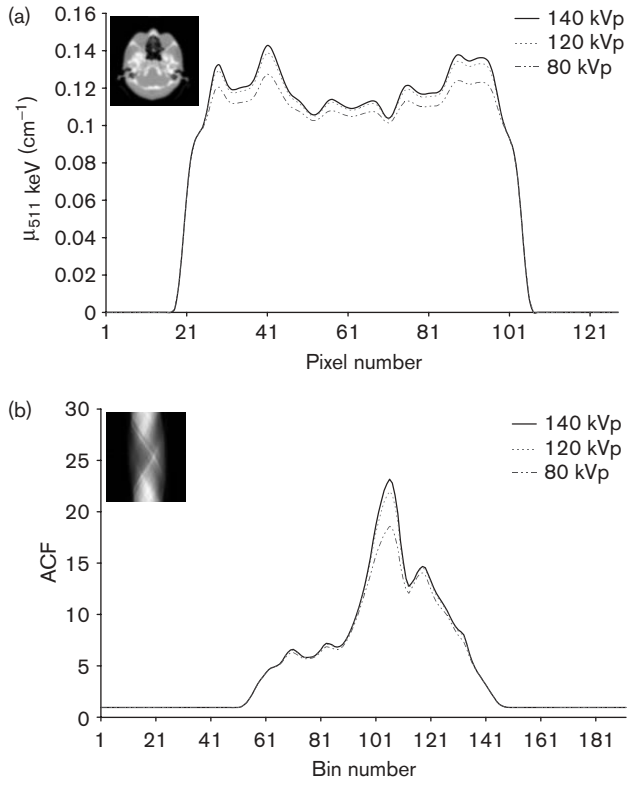

(a) Horizontal profiles through the μmaps shown in Fig. 2 and (b) central profiles through generated attenuation correction factor (ACF) sinogram (view 23/47).

benefit to the patients. Figure 3 shows the differences in the calculated μmaps and ACFs by displaying horizontal profiles through the middle of the same slice to demonstrate quantitatively the differences when using different calibration curves. Both μmaps and ACFs are overestimated when using a calibration curve derived from a tube voltage (140 kVp) higher than that used during actual CT scanning (120 kVp) of the patient. The behaviour is reversed when using a calibration curve derived from a lower tube voltage (80 kVp).

Figure 4 shows the Radiology Support Devices' striatal phantom's μmap obtained through transmission scanning using ^{137}Cs sources, as well as the μmaps calculated by CTAC when CT images were acquired at 120 kVp and scaled using calibration curves derived at different tube voltages (80, 120 and 140 kVp) and when CT images were acquired at different tube voltages (80, 120 and 140 kVp) and scaled using a single calibration curve derived at 120 kVp. The difference between the μmaps and ACFs calculated by the different methods is shown in Fig. 5. A small but noticeable difference is visible on the horizontal profiles of the ACFs as a result of the overestimation/underestimation of the attenuation coefficients depending on the combination of tube voltages used for acquisition/calibration curve derivation. The created μmaps based on the different methods (Fig. 4) were used for the attenuation correction of the emission data shown in Fig. 6. There is no visually significant difference between the images corrected for attenuation using CTAC with different combinations of tube voltages for CT image acquisition/calibration curve derivation. It should be noted that the illustrated μmaps are for different slices than the striatal images used for evaluation and shown in Fig. 6, where the differences between the μmaps generated using different conditions are small in the central region corresponding to the brain compartment (data not shown). However, the ACFs are created using three-dimensional forward projection of μmaps, and thus the noticeable differences in the bony regions might bias the ACF estimates in the striatal regions. Figure 7 shows the absolute activity concentrations estimated from the reconstructed PET images before and after partial volume correction for five individual compartments of the anthropomorphic striatal phantom. The ARCs for each compartment calculated before and after partial volume correction are also shown in Tables 1 and 2, respectively.

Fig. 4

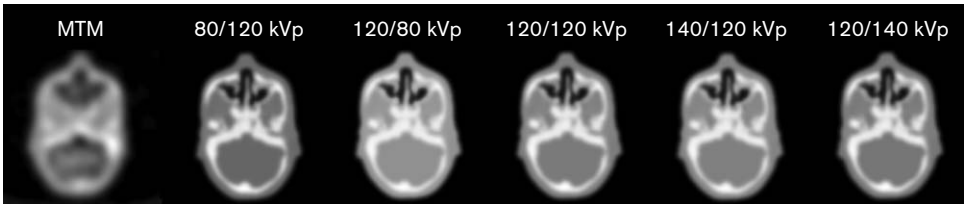

Attenuation maps at 511 keV of the anthropomorphic striatal phantom calculated using different methods. From left to right: measured transmission method (MTM) using ^{137}Cs single-photon sources; computed tomography-based attenuation correction (CTAC) method using different combinations of tube voltages for image acquisition and calculation of calibration curves.

Fig. 5

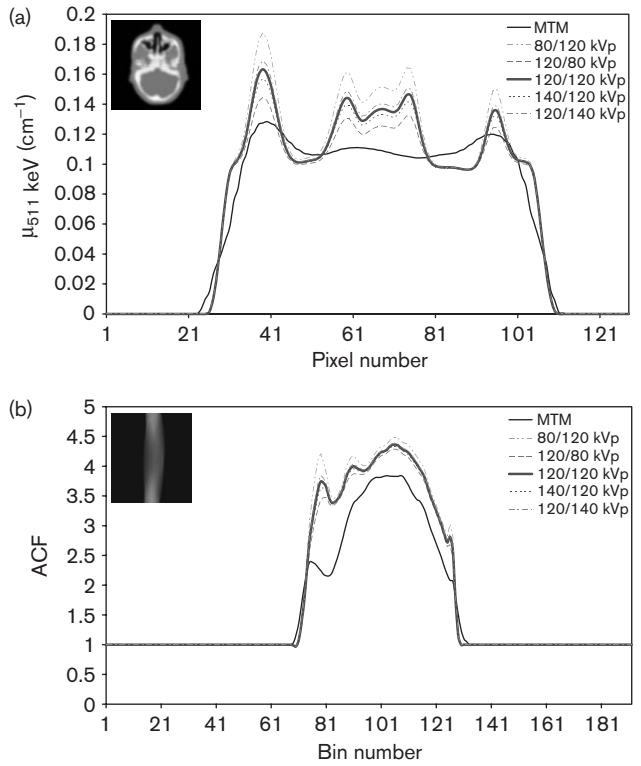

(a) Horizontal profiles through the μmaps shown in Fig. 4 and (b) central profiles through generated attenuation correction factor (ACF) sinogram (view 23/47). MTM, measured transmission method.

Discussion

The advent of dual-modality PET/CT imaging has had a strong impact on the value of diagnostic PET in the localization, evaluation and therapeutic monitoring of head and neck cancer, and may be equally valuable for other localizations that are difficult to pinpoint [18]. The decrease in the examination time as a result of the use of low-noise CT data for attenuation correction is another benefit of combined scanners. PET/CT systems have demonstrated their ability to facilitate attenuation correction using an X-ray-based patient-specific attenuation map that can be produced more rapidly and more accurately than attenuation maps generated with external radionuclide sources [2].

The general feasibility of CTAC has already been proven [10], but some practical technical issues remained to be explored. A high tube current improves CT image quality at the expense of increasing patient dose. It has been reported that effective doses of 8.81 and 18.97 mSv are delivered to the patient for a whole-body scan in high-speed and high-quality mode, respectively [19]. This is in contrast with the relatively low effective doses of 0.15 and 0.08 mSv for thoracic and whole-body transmission scans using positron-emitting ^{68}Ga/^{68}Ge and single-photon-emitting ^{137}Cs radionuclide sources, respectively [3]. This study was designed to assess the impact of using a single calibration curve on the accuracy of CTAC when CT images were acquired at different tube voltages and, vice versa, that is acquiring CT images at specific tube voltages and varying the voltage for the derivation of calibration curves. The feasibility of using a single calibration curve during practical application of CTAC for CT images acquired at different tube voltages was investigated through quantitative analysis of created μmaps, generated ACFs and reconstructed neurological PET data using experimental phantom and clinical studies. Moreover, the possibility of using low-dose CT for the purpose of attenuation correction was investigated for two commercial scanners to confirm the validity of the results reported in the literature using only clinical data (data not shown) [14]. More recently, a new pre-processing algorithm has been proposed which uses a single ultra-low-dose CT scan for both attenuation map construction and lesion localization [20].

The difference between the slopes of the calibration curves calculated at various tube voltages (Fig. 1) is due to the fact that the probability of photoelectric interaction increases with decreasing tube voltage, particularly in materials with high atomic numbers. Consequently, CT numbers in these regions increase with decreasing tube voltage. As the calculation of calibration curves is based

Fig. 6

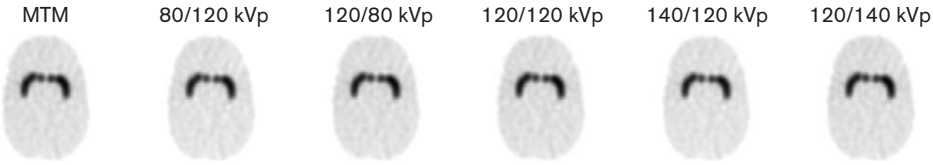

Reconstructed positron emission tomography (PET) images of the anthropomorphic striatal phantom corrected for attenuation using different methods. From left to right: measured transmission method (MTM); computed tomography-based attenuation correction (CTAC) method using different combinations of tube voltages for image acquisition and calculation of calibration curves.

on the CT numbers of air, water and cortical bone, the tube voltage dependence of the cortical bone's CT number is the reason for the difference in the slopes of the calibration curves obtained at different tube voltages. Likewise, the difference between the calibration curves at a particular tube voltage for different scanners can be explained by possible differences in detector calibration procedures, X-ray spectral shape and the reconstruction algorithms used by different scanner manufacturers. As the X-ray tube spectrum is polyenergetic, with the exact energy spectra being determined by physical factors, including the characteristics of tubes, filters, etc., the spectrum for a specific tube voltage may differ slightly between different devices. It should be emphasized that, even for a particular CT scanner and fixed tube voltage; there may be changes in calibration curves obtained at different periods of time.

The underestimation of clinical μmaps and ACFs when using a calibration curve derived at 80 kVp is due to the lower slope of the calibration curve in comparison with that obtained at 120 kVp (Figs. *2* and 3). The same behaviour was observed when using the anthropomorphic striatal phantom (Figs. 4 and 5). Generally, the difference between the μmaps and ACFs when using different calibration curves seems to be significant. The use of a calibration curve calculated at a tube voltage higher than that employed during CT scanning tends to overestimate the μmaps and ACFs. This behaviour is reversed when the calibration curve is derived at a tube voltage lower than that used during CT acquisition (Fig. 5). The underestimation of ACFs calculated by MTM, in comparison with CTAC, is the consequence of the underestimation of bone's linear attenuation coefficients at 511 keV when using low-count, low-resolution transmission scans [4,5]. In contrast, the differences between the reconstructed PET images corrected using CTAC with different combinations of tube voltages for image acquisition/calibration curves are not qualitatively (Fig. 6) or quantitatively (Fig. 7b and Table *2*) significant. One possible explanation is that the difference in ACFs varies at different projections, but is small on average. Likewise, the backprojection procedure averages the differences observed in the ACFs in projection space during the reconstruction process. The noticeable underestimation of the absolute activity concentrations (Fig. 7a) and ARCs (Table 1) for the small brain structures (LPU, RPU, LCN and RCN) within the Radiology Support Devices' striatal phantom is the result of the partial volume effect [16].

After partial volume correction of the emission images corrected for attenuation using CT images acquired at 80 and 140 kVp, average relative differences of −2.9% and 0.7%, respectively, from the images acquired at 120 kVp were observed for the absolute activity concentrations in five regions of the anthropomorphic striatal phantom when CT images were converted to μmaps using a single calibration curve derived at 120 kVp. Likewise, average relative differences of 1.9% and −0.6%, respectively, were observed when CT images acquired at 120 kVp and calibration curves derived at 80 and 140 kVp were used during CTAC. We conclude that the use of a single calibration curve for application of the CTAC procedure to images acquired at different tube voltages does not significantly affect the visual qualitative interpretation and quantitative analysis of neurological PET images.

Despite the fact that increasing tube current increases the signal-to-noise ratio and decreases the statistical fluctuations in reconstructed CT images, thus improving image quality, CT numbers and the derived attenuation maps are tube current (mA) independent (data not shown). The statistical fluctuations of CT numbers in the low-current CT images are removed during the down-sampling and smoothing procedures inherent to the CTAC procedure. Consistent with the observations reported by Kamel *et al.* [14], it appears that the tube current used during CT scanning does not affect significantly the quantification of clinical PET images for the purpose of calculating tumour uptake. As discussed above, it may happen that some slight differences are observed at the level of μmaps and ACFs when using different tube currents and a fixed tube voltage. These differences, however, will not induce significant differences during the quantitative analysis of reconstructed neurological PET images.

Fig. 7

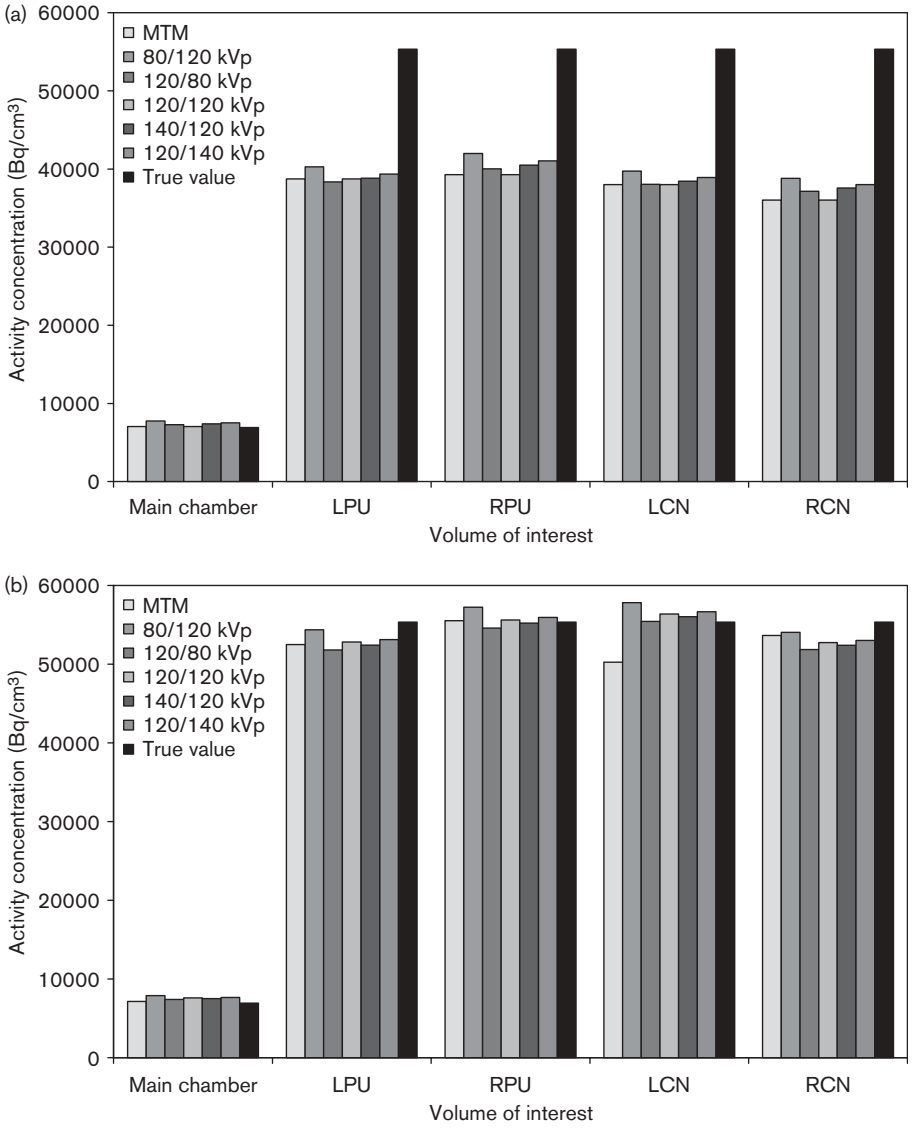

Comparison between the true and calculated absolute activity concentrations in different brain structures of the striatal phantom when using the different attenuation correction methods before (a) and after (b) partial volume correction. MTM, measured transmission method; LCN, left caudate nucleus; LPU, left putamen; RCN, right caudate nucleus; RPU, right putamen.

As this study was carried out using separate PET and CT systems for the reasons mentioned in 'Materials and methods', it was limited to the use of a neurological research brain phantom and clinical brain images, rather than an anthropomorphic whole-body phantom and whole-body clinical images, which might impose a far greater challenge to the accuracy of attenuation correction due to the much larger attenuating volume, larger bony structures and more complex juxtapositions of media with different attenuating properties, e.g. lung/soft tissue/bone in the thorax. It is hard to predict whether the answers will be equivalent or whether the same conclusions will be reached in the clinically challenging situations mentioned above. Further investigation using whole-body data is guaranteed when the inline PET/CT system becomes fully operational in our department. Given the increasing use of CT contrast media and the severe challenge that such media present for accurate attenuation correction in PET/CT, this paper does not consider the effects that might be observed in the presence of contrast media or other non-human tissue (metallic implants etc.), which are addressed in a separate paper [21].

Conclusion

The impact of the tube voltage (kVp) on the accuracy of CTAC in neurological PET studies was investigated in

Table 1 Apparent recovery coefficients for different volumes of interest (VOIs) corresponding to different structures within the anthropomorphic brain phantom before partial volume correction (α/β kVp denotes computed tomography image acquired at α kVp scaled using a calibration curve calculated at β kVp)

VOI	Volume (cm^3)	MTM (662 keV)	CTAC (80/120 kVp)	CTAC (120/80 kVp)	CTAC (120/120 kVp)	CTAC (140/120 kVp)	CTAC (120/140 kVp)
Main chamber	1290	101.74	111.87	105.00	107.79	106.76	108.62
Left putamen (LPU)	6	70.01	72.78	69.30	70.67	70.14	71.10
Right putamen (RPU)	6	71.00	75.90	72.33	73.73	73.18	74.16
Left caudate nucleus (LCN)	4.9	68.69	71.79	68.73	69.95	69.49	70.33
Right caudate nucleus (RCN)	4.9	65.08	70.10	67.14	68.32	67.87	68.69

CTAC, computed tomography-based attenuation correction; MTM, measured transmission method

Table 2 Apparent recovery coefficients for different volumes of interest (VOIs) corresponding to different structures within the anthropomorphic brain phantom after partial volume correction (α/β kVp denotes computed tomography image acquired at α kVp scaled using a calibration curve calculated at β kVp)

VOI	Volume (cm^3)	MTM (662 keV)	CTAC (80/120 kVp)	CTAC (120/80 kVp)	CTAC (120/120 kVp)	CTAC (140/120 kVp)	CTAC (120/140 kVp)
Main chamber	1290	103.36	113.83	106.76	109.63	108.58	110.49
Left putamen (LPU)	6	94.86	98.26	93.62	95.45	94.74	96.02
Right putamen (RPU)	6	96.97	103.44	98.66	100.52	99.79	101.11
Left caudate nucleus (LCN)	4.9	100.32	104.47	100.20	101.90	101.24	102.42
Right caudate nucleus (RCN)	4.9	90.79	97.68	93.73	95.31	94.70	95.80

CTAC, computed tomography-based attenuation correction; MTM, measured transmission method.

detail using experimental phantom and clinical studies. It was concluded that the application of a single calibration curve derived under standard scanning conditions during the CTAC procedure to images acquired at different tube voltages does not affect significantly the visual qualitative interpretation and quantitative analysis of neurological PET images. The same behaviour was observed when calibration curves were derived at different tube voltages and used for the conversion of CT images acquired at a fixed tube voltage. These results may contribute to alleviate the quality assurance procedures required for daily operation of PET/CT scanners in a clinical environment.

Acknowledgements

The authors would like to thank Dr O.G. Rousset for providing the PVC software and F. Schoenahl, T. Ruest and N. Andreini for their valuable support.

References

1 Townsend DW, Beyer T, Blodgett TM. PET/CT scanners: a hardware approach to image fusion. *Semin Nucl Med* 2003; **33**:193–204.
2 Hasegawa BH, Zaidi H. Dual-modality imaging: more than the sum of its components. In: Zaidi H, editor. *Quantitative analysis in nuclear medicine imaging*. New York: Springer; 2005. pp. 35–81.
3 Zaidi H, Hasegawa B. Determination of the attenuation map in emission tomography. *J Nucl Med* 2003; **44**:291–315.
4 Weinzapfel BT, Hutchins GD. Automated PET attenuation correction model for functional brain imaging. *J Nucl Med* 2001; **42**:483–491.
5 Zaidi H, Montandon ML, Slosman DO. Magnetic resonance imaging-guided attenuation and scatter corrections in three-dimensional brain positron emission tomography. *Med Phys* 2003; **30**:937–948.
6 Zaidi H, Montandon ML, Slosman DO. Attenuation compensation in cerebral 3D PET: effect of the attenuation map on absolute and relative quantitation. *Eur J Nucl Med Mol Imaging* 2004; **31**:52–63.
7 Montandon M-L, Zaidi H. Atlas-guided non-uniform attenuation correction in cerebral 3D PET imaging. *Neuroimage* 2005; **25**:278–286.
8 Beyer T, Kinahan PE, Townsend DW, Sashin D. The use of X-ray CT for attenuation correction of PET data. *Proc IEEE Nucl Sci Symp Med Imag Conf* 1994; **4**:1573–1577.
9 Kinahan PE, Hasegawa B, Beyer T. X-ray-based attenuation correction for positron emission tomography/computed tomography scanners. *Semin Nucl Med* 2003; **34**:166–179.
10 Kinahan PE, Townsend DW, Beyer T, Sashin D. Attenuation correction for a combined 3D PET/CT scanner. *Med Phys* 1998; **25**:2046–2053.
11 Burger C, Goerres G, Schoenes S, Buck A, Lonn AH, Von Schulthess GK. PET attenuation coefficients from CT images: experimental evaluation of the transformation of CT into PET 511-keV attenuation coefficients. *Eur J Nucl Med Mol Imaging* 2002; **29**:922–927.
12 Bai C, Shao L, Da Silva AJ, Zhao Z. A generalized model for the conversion from CT numbers to linear attenuation coefficients. *IEEE Trans Nucl Sci* 2003; **50**:1510–1515.
13 Guy MJ, Castellano-Smith IA, Flower MA, Flux GD, Ott RJ, Visvikis D. DETECT-dual energy transmission estimation CT for improved attenuation correction in SPECT and PET. *IEEE Trans Nucl Sci* 1998; **45**:1261–1267.
14 Kamel E, Hany TF, Burger C, Treyer V, Lonn AHR, Von Schulthess GK, *et al.* CT vs 68Ge attenuation correction in a combined PET/CT system: evaluation of the effect of lowering the CT tube current. *Eur J Nucl Med* 2002; **29**:346–350.
15 Rappoport V, Carney JPJ, Townsend DW. CT tube-voltage dependent attenuation correction scheme for PET/CT scanners. *Proc IEEE Nucl Sci Symp Med Imag Conf* 2004; **6**:3853–3857.
16 Rousset OG, Ma Y, Evans AC. Correction for partial volume effects in PET: principle and validation. *J Nucl Med* 1998; **39**:904–911.
17 Berger MJ, Hubbell JH, Seltzer SM, Chang J, Coursey JS, Sukumar R, *et al.* XCOM: photon cross sections database. NBSIR 87-3597, 1998; http://physics.nist.gov/PhysRefData/Xcom/Text/XCOM.html
18 Branstetter BF IV, Blodgett TM, Zimmer LA, Snyderman CH, Johnson JT, Raman S, *et al.* Head and neck malignancy: is PET/CT more accurate than PET or CT alone? *Radiology* 2005; **235**:580–586.
19 Wu TH, Huang YH, Lee JJS, Wang SY, Wang SC, Su CT, *et al.* Radiation exposure during transmission measurements: comparison between CT- and germanium-based techniques with a current PET scanner. *Eur J Nucl Med Mol Imaging* 2004; **31**:38–43.
20 Li J, Hsieh J, Colsher J, Stearns C, Lonn AHR. Towards single ultra-low dose CT scan for both attenuation map creation and localization in PET-CT application. *Proc IEEE Nucl Sci Symp Med Imag Conf* 2004; **4**: 2396–2398.
21 Ay MR, Zaidi H. Assessment of errors caused by x-ray scatter and use of contrast medium when using CT-based attenuation correction in PET. *Eur J Nucl Med Mol Imaging* 2006; **33**: in press.